Modeling phytoplankton blooms and inorganic carbon responses to sea-ice variability in the West Antarctic Peninsula (WAP)

C. Schultz [1,2,3], S. C. Doney [1], J. Hauck [4], M. T. Kavanaugh [5], O. Schofield [6]

[1] University of Virginia, Department of Environmental Sciences, Charlottesville, VA, USA

[2] Woods Hole Oceanographic Institution, Woods Hole, MA, USA

[3]Massachusetts Institute of Technology, Department of Earth and Atmospheric Sciences, Cambridge, MA, USA

[4] Alfred-Wegener-Institut, Helmholtz-Zentrum für Polar und Meeresforschung, Bremerhaven, Germany

[5] Oregon State University, College of Earth, Ocean, and Atmospheric Sciences, Corvallis, OR, USA

[6] Rutgers University, Center for Ocean Observing Leadership, New Brunswick, NJ, USA

Corresponding author: Cristina Schultz (cs3xm@virginia.edu)

- Longer growth season in years of early sea-ice retreat lead to higher seasonally integrated NPP, despite lower chlorophyll in January
- Sea ice is important for DIC drawdown by controlling duration of phytoplankton bloom, air-sea CO_2 fluxes and dilution by meltwater
- In the WAP, sedimentary iron has a larger role in the northern coast and shelf, glacial meltwater likely the main source in the south

Abstract

The ocean coastal-shelf-slope ecosystem west of the Antarctic Peninsula (WAP) is a biologically productive region that could potentially act as a large sink of atmospheric carbon dioxide. The duration of the sea-ice season in the WAP shows large interannual variability. However, quantifying the mechanisms by which sea ice impacts biological productivity and surface dissolved inorganic carbon (DIC) remains a challenge due to the lack of data early in the phytoplankton growth season. In this study, we implemented a circulation, sea-ice and biogeochemistry model (MITgcm-REcoM2) to study the effect of sea ice on phytoplankton blooms and surface DIC. Results were compared with satellite sea-ice and ocean color, and research ship surveys from the Palmer Long Term Ecological Research (LTER) program. The simulations suggest that the annual sea-ice cycle has an important role in the seasonal DIC drawdown. In years of early sea-ice retreat there is a longer growth season leading to larger seasonally integrated net primary production (NPP). Part of the biological uptake of DIC by phytoplankton, however, is counteracted by increased oceanic uptake of atmospheric CO_2. Despite lower seasonal NPP, years of late sea-ice retreat show larger DIC drawdown, attributed to lower air-sea CO_2 fluxes and increased dilution by sea-ice melt. The role of dissolved iron and iron limitation on WAP phytoplankton also remains a challenge due to the lack of data. The model results suggest sediments and glacial meltwater are the main sources in the coastal and shelf regions, with sediments being more influential in the northern coast.

1. Introduction

The Southern Ocean (south of 44˚S) plays a crucial role in the global carbon cycle, acting as a major sink for modern anthropogenic CO_2 and modulating, on longer time-scales, ocean-atmosphere CO_2 partitioning through variations in the biological carbon pump, surface nutrient utilization, and deep-ocean ventilation (Gruber and Doney, 2019). Contemporary air-sea CO_2 fluxes in the region reflect a combination of natural degassing to the atmosphere and

anthropogenic CO_2 uptake (Lenton et al., 2013), with the southernmost latitudes representing only a small sink. However, large-scale estimates of air-sea CO_2 fluxes do not adequately resolve the coastal regions of Antarctica, which can be highly productive biologically and act as strong sinks of anthropogenic carbon (Arrigo et al., 2008). Therefore, a better assessment of the role of the Southern Ocean in the global carbon cycle relies on improving the understanding of the air-sea fluxes and biological carbon cycling in the coastal areas of Antarctica and the fate of the excess carbon.

One of these productive coastal regions is the shelf-slope on the West Antarctic Peninsula (WAP), a sea-ice influenced marine ecosystem with relatively high primary production and net community production (NCP) during the summer season (Vernet et al., 2008; Ducklow et al., 2013; Ducklow et al., 2018), and air-sea CO_2 fluxes indicate a strong sink of atmospheric carbon (Legge et al., 2015; Jones et al., 2017). Although the dissolved inorganic carbon in the surface ocean is highly variable and controlled by a variety of physical and biological factors, such as respiration, freshwater inputs, brine rejection and mixing with subsurface waters rich in dissolved inorganic carbon (DIC; Carrillo et al., 2004; Eveleth et al., 2017), primary production is estimated to have a large role in controlling DIC during the summer months (Legge et al., 2015).

Along the WAP there are long-term trends in several physical variables, with the last decades exhibiting a substantial shortening of the sea-ice season (Stammerjohn et al., 2008; 2012), an increase in the surface ocean temperature of the order of 1˚C (Meredith et al., 2005), and melting of glaciers at an accelerating rate (Cook et al., 2005). Despite the long-term trends, the duration of the sea-ice season, as well as the intensity of the phytoplankton bloom and the surface carbon concentrations, show high interannual variability due to the influence of the Southern Annular Mode (SAM) and El Niño Southern Oscillation (ENSO) in the region (Vernet et al., 2008; Stammerjohn et al., 2008; 2012; Ducklow et al., 2013, Hauri et al., 2015). Positive phases of SAM and La Niña events lead to warmer conditions and less sea ice along the WAP, with colder years and a longer sea-ice season observed in negative SAM and El Niño years. These modes of climate variability also reinforce each other in this region, with years of

87 associated +SAM/La Niña (-SAM/El Niño) showing even warmer (colder) conditions
88 (Stammerjohn et al., 2008).
89 Understanding the mechanisms behind the variations in primary productivity and DIC in
90 the WAP is important not only to quantify its present contribution to the global carbon cycle,
91 but also to predict the changes that will occur under increased glacial meltwater input and
92 warmer conditions. Field sampling of the region, however, is limited by the presence of sea ice
93 and harsh weather during much of the year. The Palmer LTER (Long Term Ecological Research)
94 project (Ducklow et al., 2012; Ducklow et al., 2013) provides a valuable dataset that includes
95 physical, biological and chemical variables from cruises performed during the months of
96 January and February each year since 1993, but data is still limited in time to mid-summer
97 conditions. While satellite chlorophyll data helps to fill in the gaps in assessing the strength of
98 the phytoplankton blooms, the data is biased towards ice-free and non-cloudy areas, making it
99 hard to assess the timing of bloom initiation.
100 Although primary production in the WAP is patchy and can vary by an order of
101 magnitude from year-to-year (Vernet et al., 2008), some characteristics are observed
102 consistently. Phytoplankton blooms follow the retreat of sea ice, peaking first in the northern
103 and offshore areas, and there is a consistent onshore-offshore gradient, with coastal and shelf
104 waters being up to eight times more productive than offshore regions (Li et al., 2015). The
105 blooms are dominated by diatoms with secondary contributions from cryptophytes (Schofield
106 et al., 2017; Brown et al., 2019), and the main mechanism controlling its progression is thought
107 to be light limitation. Macronutrients are abundant (Kim et al., 2016) and micronutrient iron
108 limitation is not observed in the coastal areas (Carvalho et al., 2016), although it is expected in
109 the offshore regions (Arrigo et al., 2008; Li et al., 2015, Annett et al., 2017). Summer DIC
110 measurements show lower concentrations than would be expected from dilution due to
111 meltwater and glacial input, indicating that they are influenced by biological net community
112 production (Hauri et al., 2015; Legge et al., 2015).
113 Given the high interannual variability of the blooms and the patchiness observed during
114 individual years, however, the importance of different processes in controlling the timing and
115 intensity of the bloom, as well as long-term trends, remain unknown. The long-term trends in

chlorophyll based on satellite ocean color observations (decade-decade) were estimated to be negative in the northern part of the grid and positive in the southern part (Montes-Hugo et al., 2010), related to sea ice decrease, winds, and changes in mixed layer depth (MLD). With less sea ice the northern part of the WAP, where more light is available throughout the year, the region is more exposed to wind mixing, which deepens the MLD and lowers photosynthetically available radiation (PAR). In the southern WAP, areas that were previously completely covered by sea ice had an increase in PAR and higher productivity. Kim et al. (2018), however, found a trend of increase in chlorophyll values for near-shore time-series sites at Palmer Station and Potter Cove (in the northern part of the WAP), and a decrease in Rothera Station, in the southern region, driven by a sea-ice rebound that started in 2009.

While macronutrients are known to be abundant in the WAP, the concentrations of dissolved iron (dFe) and their sources are also not well constrained. It is unknown, therefore, the role dFe plays in controlling the intensity and patchiness of the bloom. This is due to the fact that collecting *in situ* seawater dFe data is a challenging process, and this micronutrient is undersampled in the WAP compared to macronutrients and biological data. Studies available, performed with relatively small datasets, reach conflicting conclusions regarding the source of dFe and how it limits primary production in different places and seasons.

Arrigo et al. (2017), using data from a late spring cruise, observed a correlation between dFe and reduced sea ice, indicating that ice melt could be a source of iron. One caveat, however, is that freshwater lenses were not linked to the higher dFe concentrations. Annett et al. (2017), using dFe and oxygen isotope data from the Palmer LTER project from 2010 to 2012, found that higher dFe concentrations were correlated with glacial freshwater content, indicating that in coastal and shelf waters glacial runoff was the major source of iron. In a study aimed at understanding the role of the Palmer Deep Canyon in providing iron to fuel phytoplankton bloom, Sherrell et al. (2018) found that high dFe was linked to sediment sources in coastal areas, which were transported to the shelf. This latter study found no connection between high dFe and glacial input, arguing that sources might differ in different locations or that vertical mixing might have muddled the interpretation of the freshwater sources in the Annett et al. (2017) study.

It has been established that lower DIC concentrations are associated with higher primary production in the late summer (Hauri et al., 2015; Legge et al., 2017), it is not clear how these two variables co-vary throughout the season. Although normalizing DIC to salinity helps to estimate the biological effect of drawdown by roughly correcting for dilution, variations in MLD change the expected end-member concentrations for DIC and salinity throughout the season through mixing with DIC-rich and more saline sub-surface waters.

In this study, we use a coupled ocean circulation, sea-ice and biogeochemistry model to fill some of the gaps in the understanding of the mechanisms controlling phytoplankton bloom and its impact on the surface DIC concentration in the WAP. We compare the model results to cruise data from the Palmer LTER project and to satellite data to validate the model results, and discuss some of the limitations from each method due to the spatial and temporal coverage.

2. Methods

2.1 Model description

The ocean circulation and sea-ice model used for this study is a regional domain version of the Massachusetts Institute of Technology General Circulation Model (MITgcm), with a hydrostatic setup that includes embedded sea-ice and ice-shelf modules. The grid used, shown in Figure 1, covers the region extending from 74.7˚S, 95˚W in the southwest to 55˚S, 55.6˚W in the northeast, with a horizontal resolution of 0.2˚ of longitude and ranging from 0.0538˚ to 0.1147˚ latitude. On the vertical, it uses z-level (fixed depth) with 50 layers spaced every 10 m for the first 120 m. The atmospheric forcings were obtained from the ERA-Interim reanalysis (Dee et al., 2011) with a horizontal resolution of 1.5˚ in latitude and longitude and a 6-hour interval. Freshwater runoff representing melt of land-based ice and iceberg calving and melting is provided with monthly climatological estimates, using the values estimated by Van Wessem et al. (2016) distributed uniformly along the coast and linearly decreasing from land out to 100 km. The grid used is shown in Figure 1, and more details on the implementation of the ocean

physical circulation and sea-ice models are described in Regan et al. (2018) and Schultz et al. (2020).

The biogeochemical model used is the Regulated Ecosystem Model version 2 (REcoM2), described in Hauck et al. (2013,2016). REcoM2 has 21 components, including two phytoplankton groups (diatoms and small phytoplankton), one zooplankton group and organic and inorganic forms of the main nutrients (iron, nitrogen, silica and carbon). Although not added as a group, bacteria functionality is represented via remineralization. Emphasis is given to phytoplankton physiology, with variable cellular stoichiometry and physiological rates that depend on the intracellular ratios of nitrogen to carbon (N:C), chlorophyll to carbon (Chl:C) and silica to carbon (Si:C). Phytoplankton chlorophyll is calculated as a function of irradiance and nitrogen assimilation, degraded at a constant rate, and lost by aggregation and grazing. A parameterization to include non-linearities in PAR due to the influence of partial sea-ice coverage was added following Long et al. (2015).

The sources of DIC are respiration, remineralization of detritus and dissolution of calcium carbonate, while sinks are fixation by primary production and formation of calcium carbonate. Alkalinity increases by nitrogen assimilation and dissolution of calcium carbonate, and decreases by remineralization and calcification. Air-sea CO_2 fluxes are calculated with code based on the Ocean Carbon-Cycle Model Intercomparison Project (OCMIP), which uses a quadratic relationship with wind based on Wanninkhof (1992). The surface CO_2 concentration is calculated at every time-step using simulated DIC, alkalinity, temperature and salinity, and the gas exchange is treated as a boundary condition for DIC.

Total dissolved iron (dFe) is assumed to be the sum of inorganic bound and organic complexed (FeL, where L is a ligand) iron. These two forms are in equilibrium according to:

$$K_{FeL} = \frac{Fe' \times L}{FeL} \quad (1)$$

where K_{FeL} is the equilibrium constant and Fe' is the concentration of free iron. Iron is added to the model via atmospheric deposition and as glacial input, and internal model sources include

respiration, remineralization (including diagenetic sediment source) and heterotrophic excretion, while sinks are represented by scavenging (proportional to detritus concentration) and photosynthesis.

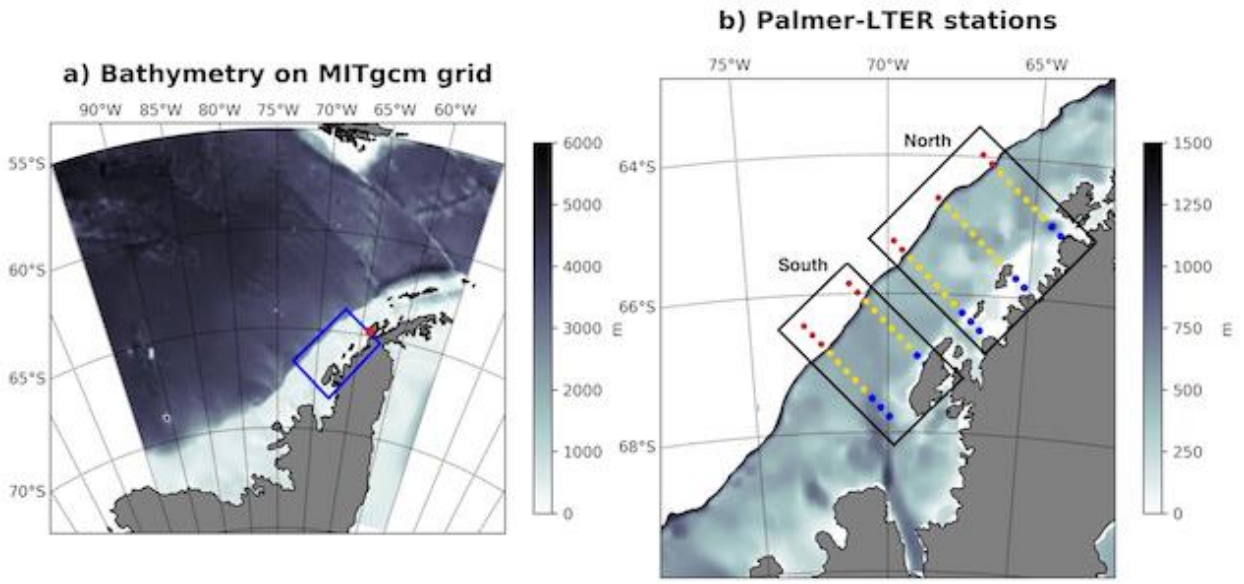

Figure 1: a) Map of model bathymetry for the full Southern Ocean sector for the West Antarctic Peninsula (WAP) with the region of Palmer-LTER cruises marked in the blue rectangle and Palmer Station marked in the red circle, and b) a larger scale map of coastal-shelf-slope (WAP) overlain with locations of the Palmer-LTER cruise sampling stations. Blue dots represent the coastal points sampled, yellow dots represent the shelf points sampled, and red dots represent the slope points sampled. The transect lines in the southern region are lines 200 (southernmost) and 300, and the transect lines in the northern region are 400, 500 and 600 (northernmost). Sub-regions analyzed are named northern coastal (n_cs), northern shelf (n_sh), northern slope (n_sl), southern coastal (s_cs), southern shelf (s_sh) and southern slope (s_sl).

2.2 Initial and boundary conditions for REcoM2

Initial and boundary conditions for dissolved inorganic nitrogen and silicate (DIN and DSi) were obtained from the World Ocean Atlas 2013, version 2 (WOA13v2, Garcia et al., 2013). Monthly climatologies were used from the surface to 500 m, with annual climatology applied

below this depth. DIC and alkalinity were obtained from the 1˚ resolution gridded Global Ocean Data Analysis Project version 2 (GLODAPv2, Key et al., 2015), with DIC representing contemporary concentrations centered in 2002 (Lauvseth et al., 2016). Atmospheric CO2 remains constant, at 380 ppm. Since dFe data is scarce, the initial and boundary conditions for this nutrient were obtained from a version of MITgcm-REcoM2 configured globally without the Arctic region, described in Hauck et al. (2016).

Atmospheric deposition and glacial sources of dFe are also represented in the model. Dust deposition is derived from the Model of Atmospheric Transport and Chemistry (MATCH), detailed in (Luo et al., 2008). Glacial inputs could be a significant source of iron to the region, but there is a lack of data on glacial concentrations of this micronutrient. Annett et al. (2017) estimated meteoric concentrations of dFe of 102 nmol/kg based on the difference of meteoric water (obtained from oxygen isotopes) and seawater dFe measurements performed between 2011 and 2012. The high concentrations are due to a source mechanism involving dFe-enriching subglacial processes and glacial meltwater streams. To avoid modifying the code, and taking advantage of the fact that input of freshwater is done at the surface, the glacial input of dFe was calculated to scale to the surface runoff at a concentration of 100 nmol/kg, but added to the same file as the atmospheric deposition. Although the glacial dFe sources include seasonal variation, a caveat of this approach is that neither glacial inputs of freshwater or dFe include interannual variability.

2.3 Experiment description

The historical physical-biogeochemical simulation builds upon an existing ocean-sea ice physical hindcast simulation with the WAP MITgcm (Schultz et al., 2020). The model physics is forced by atmospheric reanalysis at the surface, seasonally-varying glacial freshwater input from the Peninsula, and simulated ocean physics and sea-ice climatologies at the lateral boundaries from a large-scale, low-resolution circumpolar MITgcm simulation (Holland et al., 2014). Schultz et al. (2020) present a detailed assessment of the physical model behavior and skill in terms of the geographic patterns, seasonal cycle, and interannual variability ocean mixed

layer depth (MLD), sea-ice concentration (SIC) and freshwater dynamics for the WAP coastal-shelf-slope region. Overall the model performs well in capturing regional sea-ice variations from satellite observations, reflecting local thermodynamics of sea-ice formation and melt and wind-driven sea-ice advection and convergence. The model also does a credible job in simulating summertime MLD patterns found in the Palmer LTER CTD data set, though the simulated MLDs tend to be biased somewhat shallow compared to the field data. MLD reflects the complex interactions of wind-driven mixing, seasonal heating and cooling, brine rejection and sea-ice melt, and lateral circulation, and the MLD biases were improved to some extent with better model treatments of Langmuir circulation and air-sea ice drag.

The physical-biogeochemical model was integrated for 31 years, from 1984 until 2014 in a similar fashion to the physics-only simulation. The first seven years of integration (1984-1990) are considered spin-up and the results are analyzed from 1993 (first year of the summer Palmer-LTER cruises) onward. Diagnostic outputs for simulated physics, nutrients, chlorophyll, net primary production (NPP), DIC and air-sea CO_2 fluxes were saved every 5 days.

Two passive tracer experiments were conducted to assess whether sediment diagenetic sources of dFe to the water column could impact the concentration in the mixed layer. For these experiments, the climatological monthly mean fluxes of dFe from sediment to the water column were calculated, and it was determined that in the coastal and shelf waters there is a seasonal difference, with more iron being released late summer and less in the spring (Figure S1). This cycle reflects the phytoplankton bloom with an added lag, given it takes time for organic matter to reach the bottom and be remineralized. The first passive tracer experiment used a tracer that accounted for the total climatological amount of iron being released from the sea floor during the month of February. At every grid point, a diagenetic dFe concentration anomaly ($\mu mol/m^3$) was computed for the bottom layer grid cell assuming that all of sediment Fe flux ($\mu mol/m^3/d$) for the entire month of February accumulated in the bottom layer. The tracer was released at the bottom layer in the first day of February 1991, after the spin-up, and the concentration of the passive tracer was tracked during the next year. A second experiment used the same approach but using the diagenetic concentration of dFe of July, and released the tracer in the first day of July, 1991.

2.4 Calculation of DIC-derived Net Community Production (NCP)

The metabolic balance of the whole ecosystem is determined by NCP, which also governs the potential for biomass accumulation in the and carbon storage in the system. NCP is used, in this study, to assess the influence of primary production in the DIC drawdown throughout the warm season in the WAP. Since NCP is not a diagnostic variable of the model, it was calculated from the DIC drawdown between September and January. September was chosen as the start of the season since it is the earliest the phytoplankton bloom can start. For each station, the total DIC inventory for each month was calculated as the vertically integrated DIC from the September MLD to the surface. Since the mixed layer shoals during the period considered, using the September MLD guarantees that vertical mixing effects will not influence the inventory calculations performed.

The total DIC drawdown was then corrected for air-sea CO_2 fluxes and for dilution by sea-ice melt. The air-sea CO_2 flux is a diagnostic of the model, and the dilution by sea-ice melt was calculated using a salinity mixing curve. The hypothetical DIC inventory (integrated from the September MLD to the surface) at the end of the season (January) in the case where melt was the only process affecting it would be:

$$Int\_DIC_{dil} = \frac{MLD_{Sep} \times \int_{MLD}^{0} [DIC]_{Sep}}{(MLD_{Sep} + melt_{Sep-Jan})} \quad (2)$$

where MLD_{Sep} is the September MLD, $\int_{MLD}^{0} [DIC]_{Sep}$ is the vertically integrated DIC in September (from bottom of MLD to the surface), and $melt_{Sep-Jan}$ is the total sea-ice melt during the season (September to January), given in meters. For this calculation, it is assumed that sea-ice had a DIC concentration of zero. The DIC drawdown due to sea-ice melt, then, would be:

$$\Delta Int\_DIC = \int_{MLD}^{0} [DIC]_{Sep} - Int\_DIC_{dil}$$

(3)

Once corrected for atmospheric fluxes and melt, the remaining DIC drawdown is due to biological activity and therefore can be equated to NCP. The seasonally integrated (September to January) NCP, therefore is calculated as:

$$NCP_{SONDJ} = \Delta DIC_{SONDJ} - \Delta Int\_DIC - F_{CO_2}$$

(4)

where ΔDIC_{SONDJ} is the total DIC drawdown and F_{CO_2} is the air-sea CO_2 flux. The DIC-calculated NCP is then compared to NPP, which is a diagnostic variable from the model. These calculations were done for each station and averaged for each sub-region.

2.5 Data used for skill assessment

The Palmer LTER started in 1991 and has collected physical, biological and chemical data along the WAP since then (http://pal.lternet.edu/). The data include semiweekly water-column sampling near Palmer Station on the southern end of Anvers Island from October through March and an oceanographic cruise in January-February each year since 1993 (Ducklow et al., 2013). The data collected during the cruises include CTD (conductivity, temperature and depth) casts, chlorophyll-a concentration, zooplankton abundance, DIC, alkalinity and nutrients. While Palmer Station has higher temporal resolution on the data, the station data is more affected by islands, near-shore bathymetry and synoptic scale phenomena that are not captured by the model. The cruise sampling grid is too coarse to resolve mesoscale features given the short Rossby radius on the shelf, a conclusion that is supported by studies using underway data from Palmer LTER cruises (Eveleth et al., 2017). Individual sampling stations can also be affected by

phenomena such as the passage of icebergs, which will not be captured by the model. Clustering the cruise stations in sub-regions and calculating the climatological values and their anomalies makes it more likely that the data will represent the seasonal variations at a larger spatial scale; and could therefore be more accurately compared to the model data.

This study uses data from lines 200 to 600 of the Palmer LTER grid, spanning 500 km along the coast and 250 km across the shelf. As shown in Figure 1b, the across-shelf transects are separated by 100 km, with stations 20 km apart in each transect. All the data is available on the project web page (http://pal.lter.edu/data/). Not all stations are sampled for all variables measured by the project each year, and each measurement does not necessarily reflect the mean state of the water column during the summer. To decrease the influence of short-term and small-scale processes, the cruise data was divided in north (lines 400 to 600) and south (lines 200 and 300) regions, and into coastal, shelf and slope regions, based on bathymetry. Six different regions are therefore analyzed: northern coastal (n_cs), northern shelf (n_sh), northern slope (n_sl), southern coastal (s_cs), southern shelf (s_sh) and southern slope (s_sl).

Level 2 remote sensing reflectances (Rrs) from Aqua-MODIS (v. 2018) and SeaWiFs (v.2018) spanning 1997- 2018 were downloaded from NASA Goddard and binned to a common 10 km grid (Kavanaugh et al., 2015). Chlorophyll-a concentration was calculated per image using an algorithm tuned specifically for the WAP (Dierssen and Smith, 2000). While this algorithm was tested during SeaWiFs era, the superior skill has been confirmed with vicarious comparisons using 1 km Aqua-MODIS data and modern in situ chlorophyll-a from recent Palmer LTER station and cruise data (Kavanaugh et al., 2015). As the WAP can experience multiple overflights per day, a daily composite was calculated over the grid, from which an 8 -day and monthly averages was calculated using geometric means. SeaWiFs and MODIS time series were merged using the method of Kavanaugh (et al., 2018), which applies a per-pixel seasonal correction to SeaWiFs data.

Sea-ice satellite images are obtained from GSFC (Goddard Space Flight Center) Bootstrap algorithm (Comiso, 2017). Climatological and monthly mean sea-ice concentration (SIC) are calculated from binned 8-day means with horizontal resolution of 0.2 degrees in latitude and longitude. Onset time of sea-ice advance is chosen to be the day in which the

361 average SIC of all the stations in each Palmer LTER sub-region reaches at least 0.15 (15% of the
362 area covered by sea ice) for 5 days in a row. Sea-ice retreat is assumed to be the last day in
363 which SIC is greater than 0.15 for the ice season. Further details are provided in Stammerjohn
364 (2008; 2012).
365
366 **3 Results**
367
368 **3.5 Iron sources in the model**
369
370 Given the low temporal and spatial coverage of available in situ dFe data, questions
371 regarding the mechanisms that supply this micronutrient to different regions in the WAP, as
372 well as how limiting iron is to primary production, still persist. While Arrigo et al. (2017) argues
373 that sea ice could be a major source during early spring, Annett et al (2017) found that glacial
374 meltwater was associated with higher dFe and Sherrell et al. (2018) found that dFe in coastal
375 areas was supplied by sediment sources near Palmer Deep canyon.
376 In the model, atmospheric deposition of iron is negligible, and the sources of dFe to the
377 mixed layer are glacial input, entrainment from below the mixed layer or transport from other
378 locations, including from the bottom layer which is enriched via sediment diagenetic processes.
379 The glacial source of dFe is prescribed; climatological estimates of freshwater runoff were
380 uniformly distributed along the coast and decreasing linearly in volume from the shore out to
381 100 km from the coast, and a concentration of 100 nM of dFe was added to this runoff. The
382 entrainment from below the mixed layer was calculated from the monthly climatology using
383 the equation:
384

$$F_{ent} = \frac{dMLD}{dt}\Delta[dFe] \quad (5)$$

385
386 where dMLD/dt is the deepening of the MLD from month to month and $\Delta[dFe]$ is the dFe
387 concentration difference between the mixed layer and the layer below. Equation 2 is only valid
388 for periods of deepening mixed layer, since the subsurface dFe concentrations are consistently

higher than the concentrations in the mixed layer. The fluxes during shoaling periods were set to zero, since no dFe was added to the mixed layer. Estimating the influence of sediment dFe at a certain location is more difficult given the role of circulation and transformation processes while iron makes its way from the sediment to the mixed layer. Using the concentration of the passive tracer experiments described in the Methods (Section 2.3) can give us an idea of where this source could be significant, but quantifying how much dFe comes from the sediment is not the goal of this experiment given that, unlike a passive tracer, iron could be consumed and transformed along the way from the sediment to the sub-regions of interest.

Figure 2 shows the flux of glacial and entrainment sources to the mixed layer (in orange, red), and the concentration of passive tracers in the ML during the year following their release (in black). Diagenetic dFe is a major source only in the northern coastal region, having a smaller impact in the southern coast and northern shelf, and no impact in the southern shelf and slope regions. Glacial sources, as expected from the design of the forcing files, has diminishing importance from the coast to the slope areas. Entrainment from below the mixed layer is a source of iron from late summer to early spring in the shelf and slope, but this mechanism of iron enrichment is halted from September through January while the mixed layer shoals.

This analysis shows that there is an (expected) difference in terms of iron supply between coastal, shelf and slope areas, but also that there is a difference between the northern and southern regions, stronger in the coastal region. The model results indicate that in the northern coastal area, which is shallower and more influenced by circulation around the islands, sedimentary processes are major source of dFe, while in the south glacial input is the dominant source of dFe. This difference validates the hypothesis suggested in Sherrell et al. (2018) that the discrepancies found between their study and the study of Annett et al. (2017) could be due to different sources having different impacts throughout the WAP. While Annett et al. (2017) found the highest correlations between meteoric water and dFe in the southern part of the grid, the study of Sherrell et al. (2018) was aimed at understanding Palmer Deep, located near-shore and closest to line 600 (north).

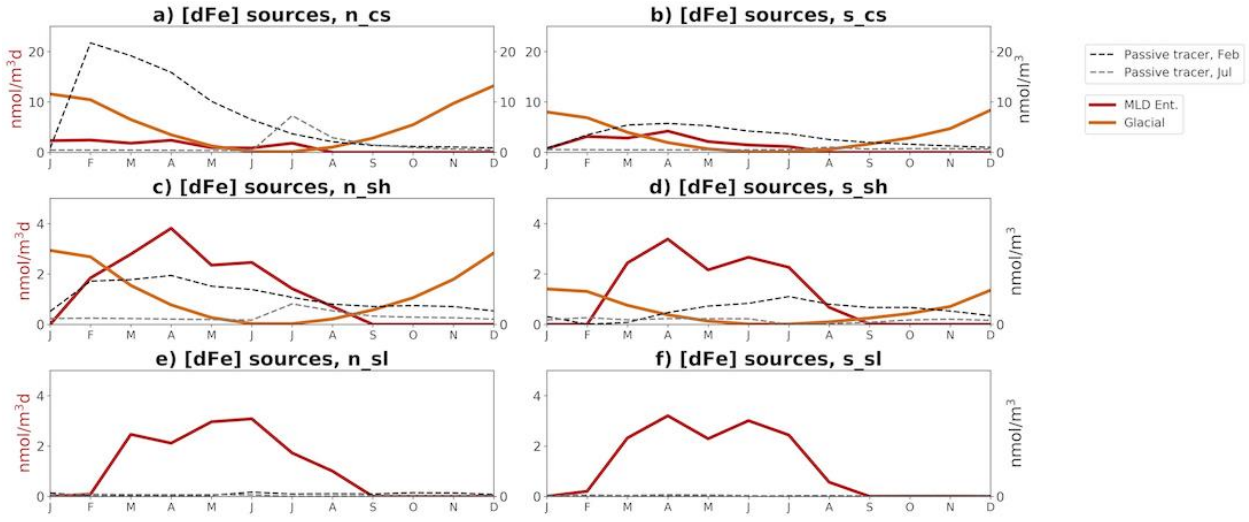

Figure 2: MITgcm-REcoM simulated glacial fluxes of dFe (orange), dFe entrainment from below the ML (red) in nmol/m^3d (y-axis scale on the left of plot). Dotted lines in black and gray represent the concentration of passive tracers (January and July, respectively) released at the bottom in the mixed layer of each sub-region in the year following their release (y-axis scale on the right of plot). Notice the different y-axis scales for coastal region compared to shelf and slope regions.

While we suspect that the subsurface concentration of dFe in the model is higher offshore than would be observed due to the values used for the initial and boundary conditions, there is no data to validate this assumption. There are also significant uncertainties about the transformation and scavenging rates for dFe along the WAP. If the mechanisms represented in the model are correct, however, the higher iron concentrations found in regions of low sea ice in the slope regions, as found in Arrigo et al. (2008), would be explained by the fact that low sea ice concentration promotes mixing of surface waters with iron-rich subsurface waters by enhancing wind action, not due to iron released from sea ice.

3.6 Model skill in reproducing phytoplankton bloom climatology

To assess the model skill in reproducing the observed bloom climatology, we compared the monthly mean surface chlorophyll concentrations and SIC from the model with the monthly mean satellite data, shown for the period between November and February in Figure 2. Similar to observations, the simulated progression of the bloom follows the retreat of sea ice from offshore to onshore and from north to south. In parts of the grid, particularly the southern shelf and slope, however, the start of the bloom happens later in the model due to a delay in the modeled sea-ice retreat in this region, which leads to lower PAR at the beginning of the season.

The model also simulates the onshore-offshore gradient in surface chlorophyll seen in the observations, with higher concentration in the coastal and shelf areas. The simulated chlorophyll, however, has higher values in the coast and shelf regions in December and in the offshore areas throughout the season. It is thought that primary production offshore is limited by iron (Garibotti et al., 2005), which is not the case in the model as can be seen in the seasonal progression of the limitation terms, shown in Figure S2. Given the lack of iron data in the region, particularly farther from the coast, the understanding of the iron dynamics is limited and it is not possible to derive initial and boundary conditions from observations. Therefore, it is possible that the model derived subsurface dFe, which reaches concentrations of 0.75 µmol/m3 in all sub-regions, is too high; leading to the higher chlorophyll values. The model also shows a sharper decrease in chlorophyll from January to February compared to the satellite data.

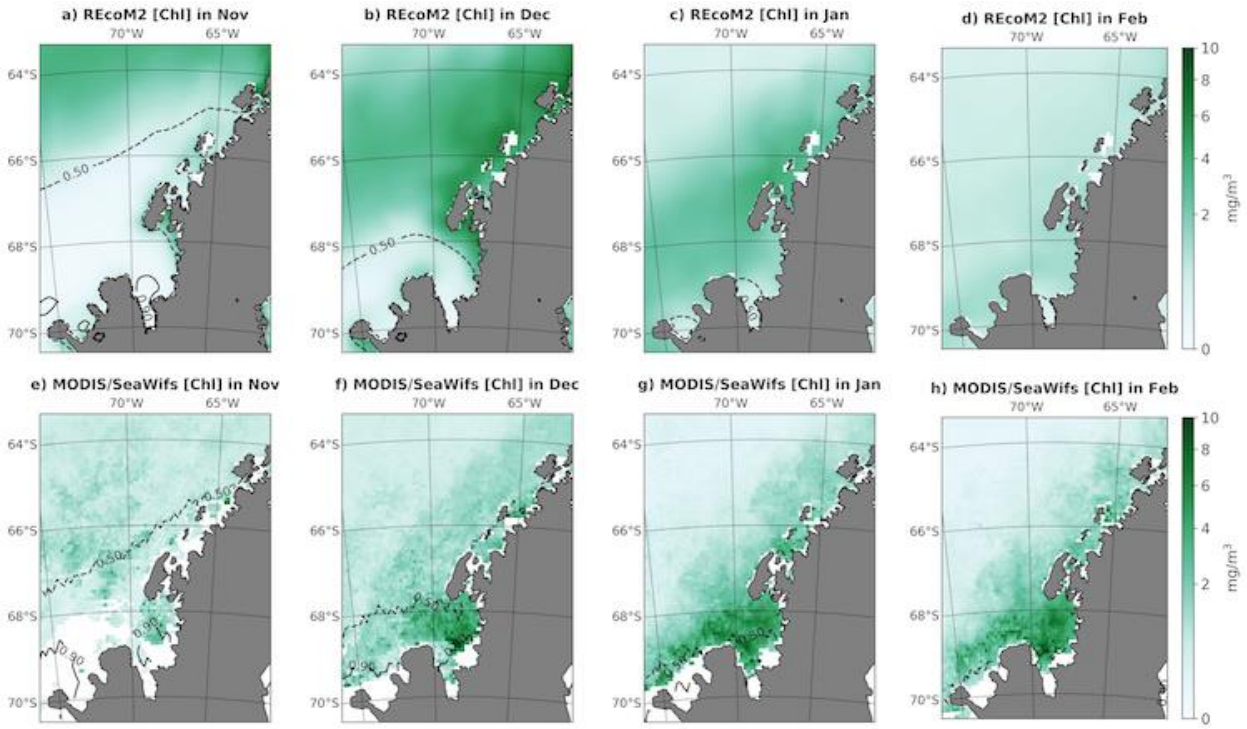

Figure 3: MITgcm-REcoM2 (top) and MODIS/SeaWifs (bottom) climatological surface chlorophyll concentration for November, December, January and February (left to right). Black dashed line shows SIC equal 0.5, and black full lines show SIC of 0.9

For each Palmer LTER survey cruise station, the data from the nearest model and satellite grid points were extracted, and the evolution of the surface chlorophyll concentrations and SIC are shown in Figure 4 along with the Palmer LTER surface chlorophyll data, assumed to be the January mean. Although the Palmer LTER data only has one data point per station each year, making it hard to assess whether each data point it is representative of the regional values for that year, the climatological mean (calculated as the geometric mean of all the stations for each sub-region between 1993-2014) is comparable to the satellite climatology. The Palmer LTER and satellite data are similar in the northern region, while in the south the satellite shows slightly higher surface chlorophyll concentrations.

From Figure 4 it is also seen that simulated January chlorophyll concentrations are closer to the observed values in the coastal regions, particularly in the southern coast where

sea-ice advance and retreat is better represented. Although the simulated bloom starts later than observed in the satellite data, the timing of the peak of the bloom coincides with the observations in much of the grid, with the exception of the southern coast and slope. The model chlorophyll values also show the lowest summer values in February, with increased concentrations in March. Given that PAR availability in March is lower than in February, this can be attributed to iron limitation. The iron limitation terms are lowest in January, indicating high consumption during this month and leading to lower chlorophyll concentrations in early February before iron is replenished by deepening of the mixed layer.

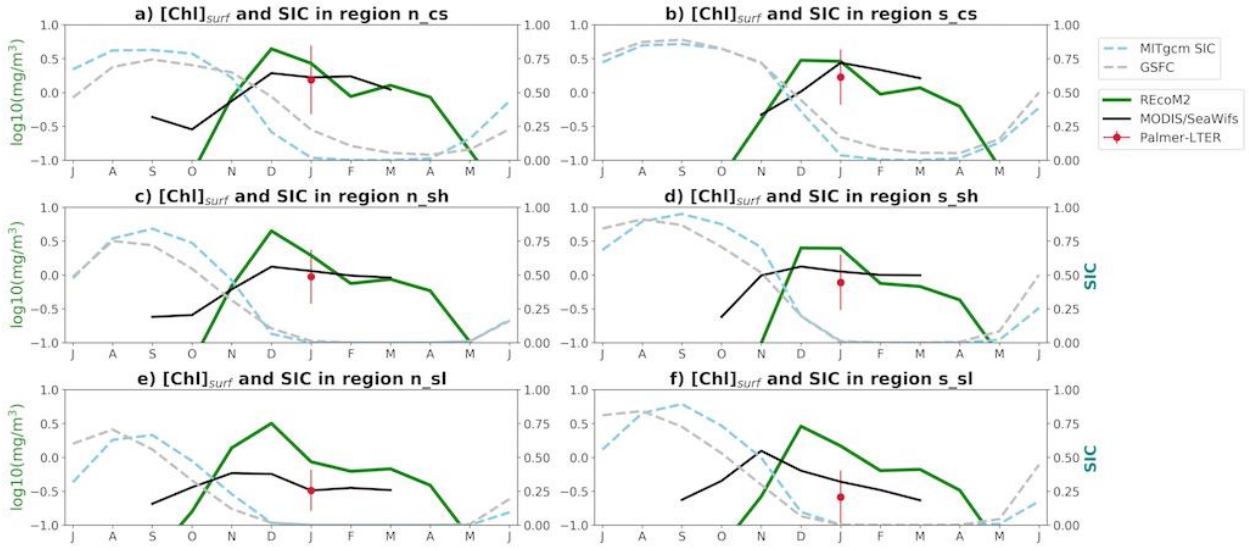

Figure 4: MITgcm-REcoM2 (light blue dashed line) and GSFC (gray dashed line) climatological monthly sea ice concentration; MITgcm-REcoM2 (green) and MODIS/SeaWifs (black) log-transformed climatological monthly surface chlorophyll concentration; Palmer-LTER $\log_{10}$-transformed climatological surface chlorophyll concentration (red dot, plotted as January mean), during July-June, for regions n_cs (a), s_cs (b), n_sh (c), s_sh (d), n_sl (e), s_sl (f). Vertical lines represent standard deviation.

3.7 Interannual variability of the phytoplankton bloom

To analyze the interannual variability of the phytoplankton bloom, the anomalies (relative to the climatology) of surface chlorophyll concentration were calculated for each sub-

region and for each dataset (Figure 5). For this comparison, the January monthly means were used for the satellite and model data, and the reference period from which the anomaly was calculated was from 1998, when satellite measurements started, until 2014. The figure shows discrepancies among the datasets, which could be attributed to the limited data collection and the patchiness of the bloom.

Retreat of sea-ice can be early during some sub-regions and late in others (Figure S3), depending on temperature and wind patterns throughout the season. Sea-ice ridging in the coastal areas can happen as sea-ice gets pushed from the slope and shelf areas. In the years in which sea-ice retreat happened consistently early in all sub-regions, such as 1999 and 2009, surface chlorophyll anomalies were mostly negative or close to neutral in all datasets, while years of consistent late sea-ice retreat like 2005 and 2014 showed mostly positive or low negative anomalies. The exception for this pattern is coastal chlorophyll anomalies from the MODIS/SeaWifs dataset in 2005, which showed negative anomalies. In 2005, however, satellite images were scarce in the coastal region (1 in the northern coast and 4 in the southern coast), and it is possible that the satellite data missed the peak of the bloom during this season.

It is also worth noting that one of the limitations of the model is that it does not have interannual variability in the glacial discharge. This could be the cause of the lower chlorophyll concentrations simulated in some of the years in which satellite and cruise data show large blooms, such as 2006 and 2011. The year 2011 is one of the only years for which dFe data is available, and Annett et al. (2017) found that this year had much larger dFe and glacial meltwater concentrations compared to 2010 and 2012, particularly in the southern region, leading to an anomalously productive season. This was also a year of anomalously early sea-ice retreat, which would otherwise lead to an early bloom and deeper MLD in January, usually indicative of lower chlorophyll concentrations during this month.

Although there are marked differences between the MODIS/SeaWifs and Palmer LTER data, the correlations in time (using the January means for satellite and model data, and cruise data) calculated for the surface chlorophyll for each sub-region range from 0.52 in the northern slope to 0.73 in the southern shelf and are larger than the correlations between these datasets and the model data (Table S1). The only significant correlation for the simulated data was with

the Palmer-LTER data in the northern coast (0.57). In years in which all sub-regions showed anomalous early or late sea-ice retreat (Figure S3), however, there was agreement between the datasets on whether this was a high or low chlorophyll year in January. The seasons of 1998-1999 and 2008-2009 were chosen to represent years of early sea-ice retreat, with negative chlorophyll anomalies in all datasets; and 2004-2005 and 2013-2014 were chosen to represent years of late sea-ice retreat, with positive chlorophyll anomalies. Although 2011 also showed early sea-ice retreat, it was not considered in analyses in the next sections due to the anomalously high dFe observed, which would mean it does not necessarily represent the mechanisms that took place during the other low-ice years.

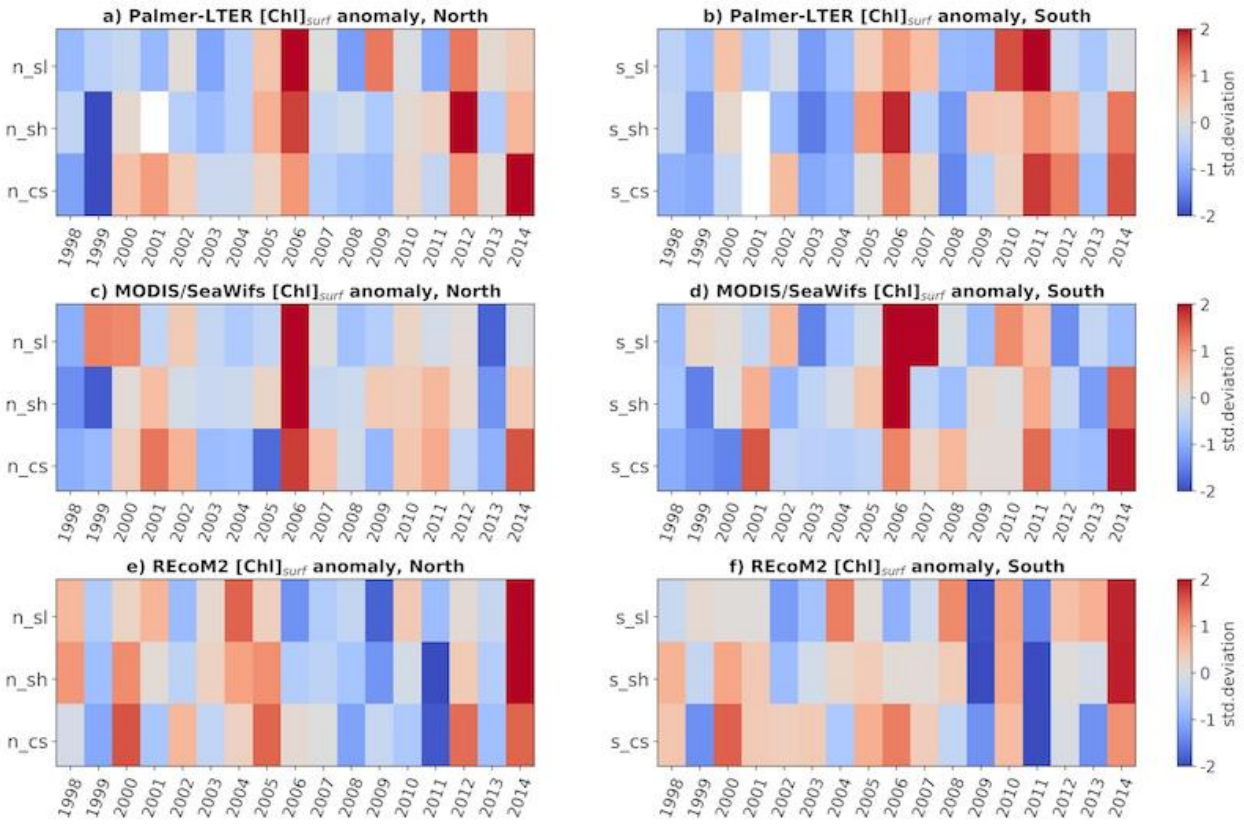

Figure 5: Surface chlorophyll concentration anomalies, relative to the cruise climatology for Palmer-LTER data (a,b), and relative to January climatology for MODIS/SeaWifs (c, d) and MITgcm-REcoM2 (e, f); for northern region (a, c, e) and southern region (b, d, f).

3.8 Phytoplankton blooms in seasons of early and late sea-ice retreat

To compare the differences between years of early sea-ice retreat and the climatology, the monthly geometric mean surface chlorophyll concentration for the early sea-ice retreat seasons (1998-1999, 2008-2009) were calculated for the satellite and model data and plotted against the monthly climatology (Figure 6). The Palmer LTER data is considered as a January mean, and is also plotted in the same figure. The model output suggests an earlier bloom compared to the climatology in the years of early sea-ice retreat. In the satellite data, this trend is observed in the slope region, and hard to determine in the coastal region given the lack of data during the spring and early summer.

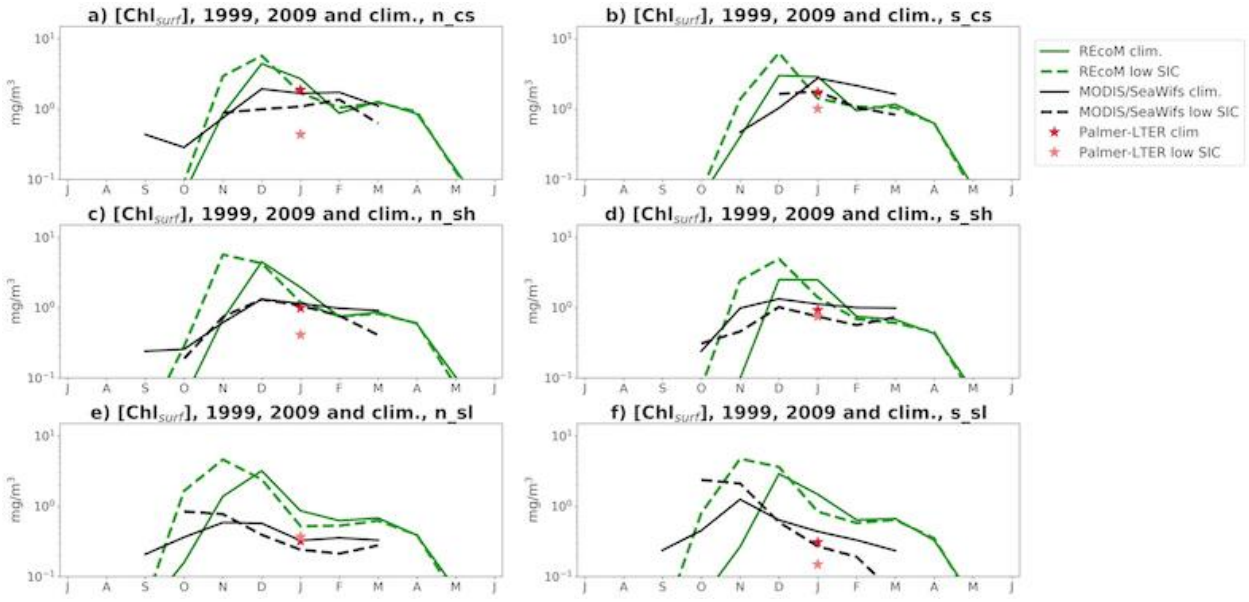

Figure 6: MITgcm-REcoM2 (green) and MODIS/SeaWifs (black) $\log_{10}$-transformed climatological monthly surface chlorophyll concentration (full line) and mean concentration for years of early sea ice retreat (dashed line); Palmer-LTER log-transformed climatological surface chlorophyll concentration (red star, plotted as January mean) and mean for years of early sea ice retreat (pink star), during July-June, for regions n_cs (a), s_cs (b), n_sh (c), s_sh (d), n_sl (e), s_sl (f).

By January, however, all datasets agree that surface chlorophyll concentrations are generally lower than the climatological values, with exception being that Palmer LTER shows slightly higher concentrations in the northern slope and the satellite data has similar values to the climatology in the northern shelf. In the model, lower chlorophyll values in January can be attributed to iron limitation, given that an earlier bloom leads to earlier depletion (Figure S2). Although the model tends to underestimate MLD (Schultz et al., 2020), the time at which light limitation is lifted, associated with the sea-ice retreat, is well represented. It is possible that the higher chlorophyll values (compared to observations) seen in the model are partially fueled by less light limitation at the bottom of the mixed layer. In 2011, however, deeper than usual MLD due to very early sea-ice retreat was observed in the coastal and shelf areas during the Palmer LTER cruise (Schultz et al., 2020), associated with high chlorophyll and dFe concentrations (Annett et al., 2017). This indicates that although light limitation has a large role in controlling the timing of the bloom, there is enough PAR in mid-summer to fuel large primary production even in years of anomalously deep mixed layer, and iron limitation could be the reason for the lower concentrations observed.

During the years of late sea-ice retreat (2004-2005,2013-2014, Figure 7) it is hard to determine the time of the start of the bloom in the satellite data, given that chlorophyll cannot be observed earlier in the season due to sea-ice cover. During December and January, however, the satellite data shows that chlorophyll concentrations are higher than their climatologies in the coastal region and southern shelf, with values similar to the climatology in the northern shelf and lower concentrations in the slope region. The Palmer-LTER and model data indicate higher chlorophyll in all sub-regions by January. In the model, this is due to a late start of the bloom, leading to a later peak.

Overall, despite disagreements in the mean chlorophyll values, all the datasets agree that the years with early sea-ice retreat had lower chlorophyll concentrations in January while late sea-ice retreat leads to higher chlorophyll concentrations. While difficult to assess the progression of the bloom in each set of years from the satellite and cruise data, the model indicates that less sea ice leads to an earlier bloom and less dFe available by January, with the opposite happening in years of increased sea ice. While the timing of the bloom is dictated by

PAR limitation, the summer concentrations depend on how much dFe has been consumed earlier in the season.

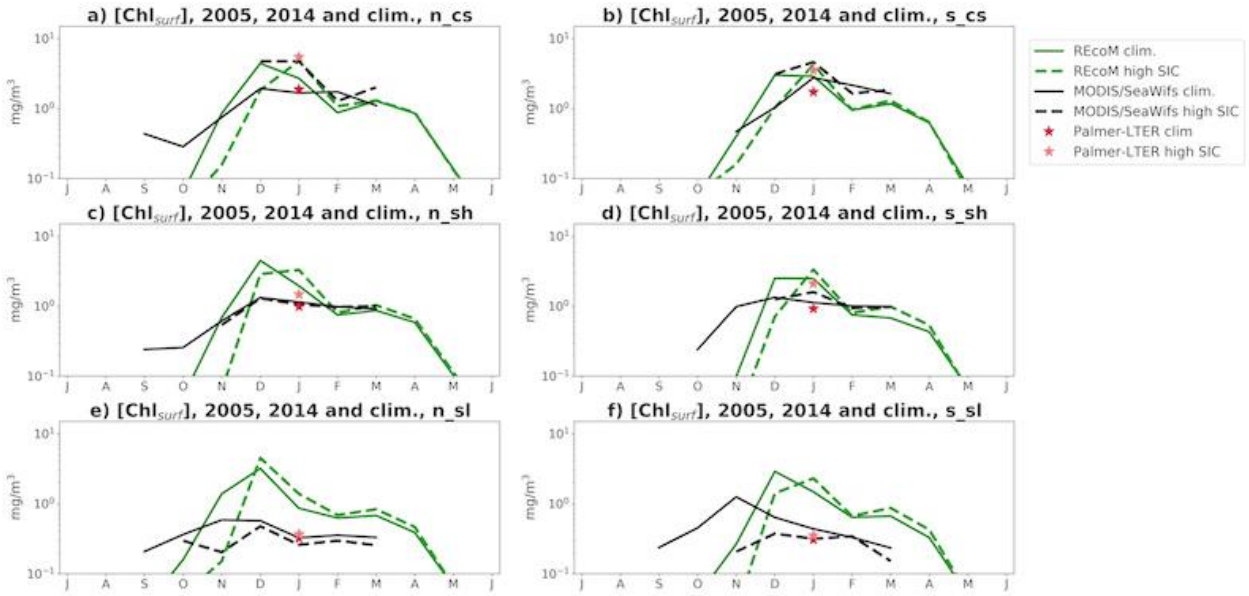

Figure 7: MITgcm-REcoM2 (green) and MODIS/SeaWifs (black) $\log_{10}$-transformed climatological monthly surface chlorophyll concentration (full line) and mean concentration for years of late sea-ice retreat (dashed line); Palmer-LTER $\log_{10}$-transformed climatological surface chlorophyll concentration (red star, plotted as January mean) and mean for years of early sea-ice retreat (pink star), during July-June, for regions n_cs (a), s_cs (b), n_sh (c), s_sh (d), n_sl (e), s_sl (f). Vertical lines represent standard deviation.

3.9 Spatial distribution and interannual variability of DIC

January monthly mean surface DIC concentrations from the model output were compared to the Palmer LTER cruise data (Figure 8), with the anomalies relative to the climatology for each sub-region also shown. The model is able to capture the onshore-offshore DIC gradient seen in the observations, with lower concentrations towards the coast (Hauri et al., 2015). However, the simulated values have a bias towards lower concentrations compared to the cruise data. There are a few limitations in the model that could explain the low bias, one

of them being that freshwater inputs are added at the surface, which could lead to less mixing and lower DIC from dilution. Also, the initial and boundary conditions are based on gridded datasets that are derived from observations mostly collected in open-ocean locations, and Jones et al. (2017) found that DIC concentrations in Antarctic Circumpolar Water (ACC) derived water masses were higher in the shelf due to respiration and remineralization as the water mass makes its way from the slope to the coast. A third reason that could explain the bias towards lower DIC is that a bias towards higher NPP observed in the model results, which could also reflect higher net community production and carbon uptake.

Despite a bias towards lower concentrations, the interannual variability of simulated DIC is similar to the variability observed in the Palmer LTER cruise data in most regions, with the exception of the southern slope (Table S2). DIC variations throughout the season are influenced by a series of physical and biological mechanisms (Ducklow et al., 2018). The variability of the physical mechanisms that affect DIC concentrations, which are deepening of the MLD (which leads to entrainment of high-DIC sub-surface waters) and sea ice melt (which leads to dilution), are well represented in the model (Schultz et al., 2020). Although the phytoplankton bloom is patchy and chlorophyll concentration may vary throughout the season at a certain location, the biological signature of net community production carbon uptake lasts throughout the growth season (September to the Palmer LTER survey cruise in January). Therefore, the better agreement between simulated and cruise DIC values compared to the chlorophyll concentration adds to the evidence that part of the disagreement between the chlorophyll datasets is due to the patchiness of the data, and that integrated over the season, the biological processes are better represented in the model.

Some of the discrepancies between simulated and cruise DIC are likely to be due to the same mechanisms as the discrepancies in the chlorophyll values. In 2011, the model is not capable of capturing the large bloom observed, leading to positive DIC anomalies in the southern region while the cruise data shows negative anomalies. For the years of early sea-ice retreat analyzed, both REcoM2 and Palmer-LTER data show positive DIC anomalies, while for the years of late sea-ice retreat the anomalies are mostly negative with the exception of the slope region.

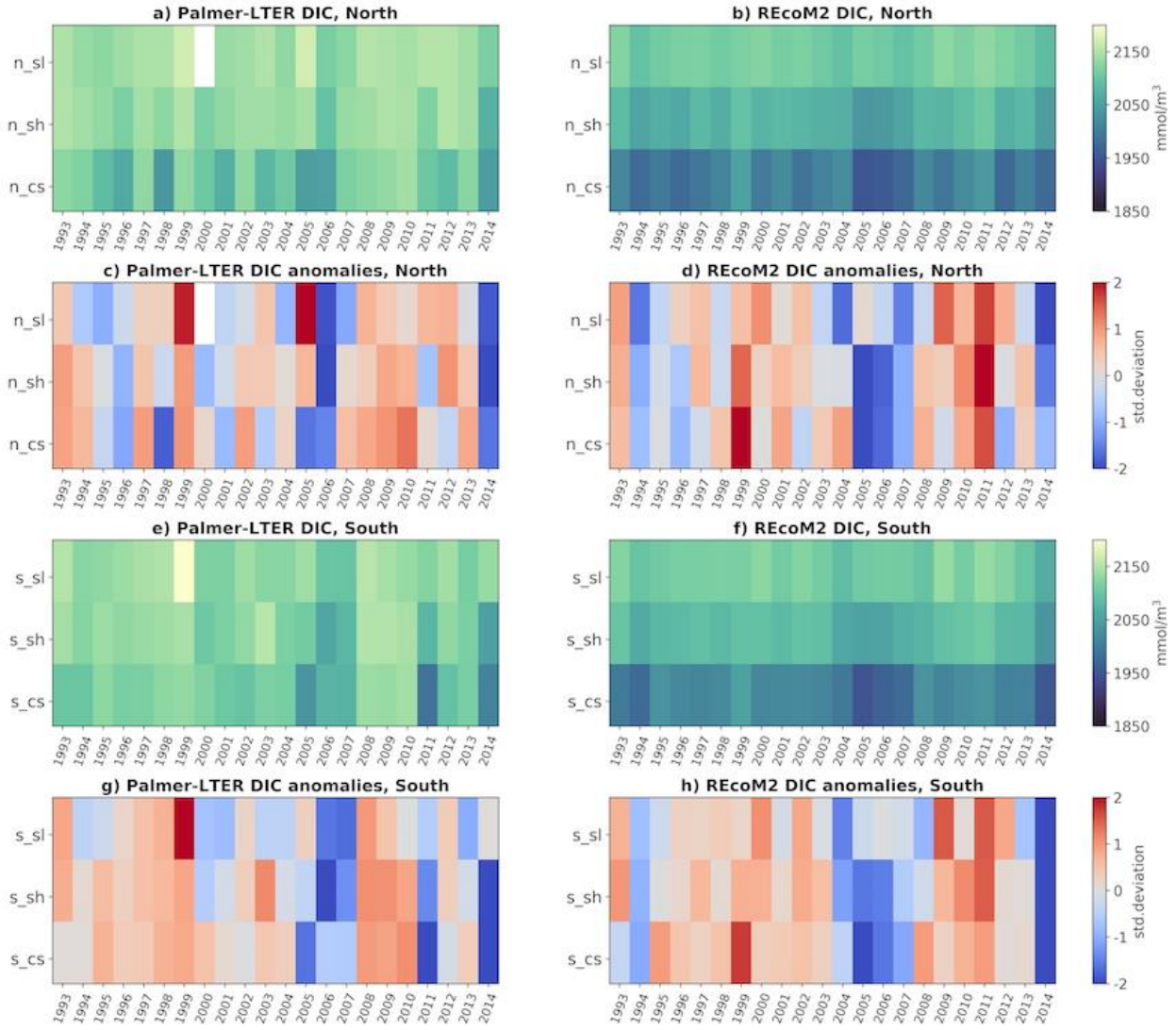

Figure 8: Palmer-LTER (left) and MITgcm-REcoM2 (right) January surface DIC concentrations (a, b, e, f) for north (a, b) and south (e, f) regions; and anomalies relative to the mean (January mean for simulated, and cruise mean for Palmer-LTER, c, d, g, h).

3.10 DIC-derived Net Community Production

Although the DIC anomalies provide an indication of the physical and biological processes that took place throughout the growth season, further quantification is needed to

649 assess how much of the DIC drawdown is due to net biological uptake, air-sea fluxes and sea ice
650 melt. The calculations described in section 2.4 provide an estimate of the influence of each of
651 these processes in the DIC, and the total DIC drawdown, air-sea CO2 fluxes, DIC dilution due to
652 sea ice melt, NCP and seasonally integrated NPP (a diagnostic variable) are shown, for each sub-
653 region, on Figure 9. January NPP is shown in Figure S5. All these figures include the calculations
654 for the climatology and for the years of early and late sea-ice retreat described in previous
655 sections.
656 In a study using Palmer LTER cruise data, Ducklow et al. (2018) find that NCP is
657 significantly higher than measured export flux, a conclusion that is also reached by other
658 studies (Buessler et al., 2010; Weston et al., 2013; Stukel et al.,2015). Within each year
659 sampled, the variability of each rate process measured, including NCP, was moderately high in
660 both space and time and production likely being higher in sunny days (versus cloudy
661 conditions). The authors also point out that one of the big uncertainties in trying to assess the
662 relative magnitude of each estimates is the difficulty in specifying the start of the growing
663 season after sea-ice retreats.
664 Total DIC drawdown is highest in the northern shelf and coastal areas during years of
665 late sea-ice retreat, compared to the climatology and to years of early sea-ice retreat (Figure 9
666 a,b). This happens despite NCP being higher in years of early sea-ice retreat throughout the
667 whole grid (Figure 9 g,h). The largest drawdown was observed in the northern coast, with a
668 climatological decrease of 4.16 molC/m^2 during the season that reached 4.74 molC/m^2 during
669 years of late sea-ice retreat. Higher NCP in years of low SIC is consistent with the satellite
670 estimates of Li et al. (2015), who found that variations in NCP were linked to sea ice, and that
671 annually integrated NCP was higher with higher sea surface temperature and longer bloom
672 season. The larger DIC drawdown despite lower NCP indicates a strong influence of physics in
673 the inorganic carbon cycle. With increased sea ice throughout the season, there is less air-sea
674 transfers (which are a source of DIC) and more dilution by late summer.
675 In previous studies using Palmer LTER cruise data, Hauri et al. (2015) found that DIC was
676 driven by increased biological activity in the south of the WAP and by increased meltwater
677 towards the north, and Eveleth et al. (2017) found that physical processes had a more

pronounced influence in the southern onshore region where active sea-ice melt was still happening. The model results show that although climatological summer meltwater values (December to February) are higher in the southern part of the grid (Schultz, et al.,2020), integrated over spring and summer sea-ice melt has a larger influence in the northern WAP in years of late sea-ice retreat, and larger influence in the southern part in years of early sea ice retreat (Figure 9 e, f). The calculation performed to account for the influence of meltwater takes into account the depth of the MLD, which is shallower in the northern part of the grid (Schultz et al., 2020), increasing the effect of melt. Both sea-ice melt and primary production tend to be higher in the southern part of the grid by January and February when the Palmer LTER cruise takes place, but the relative importance of each process varies from year to year.

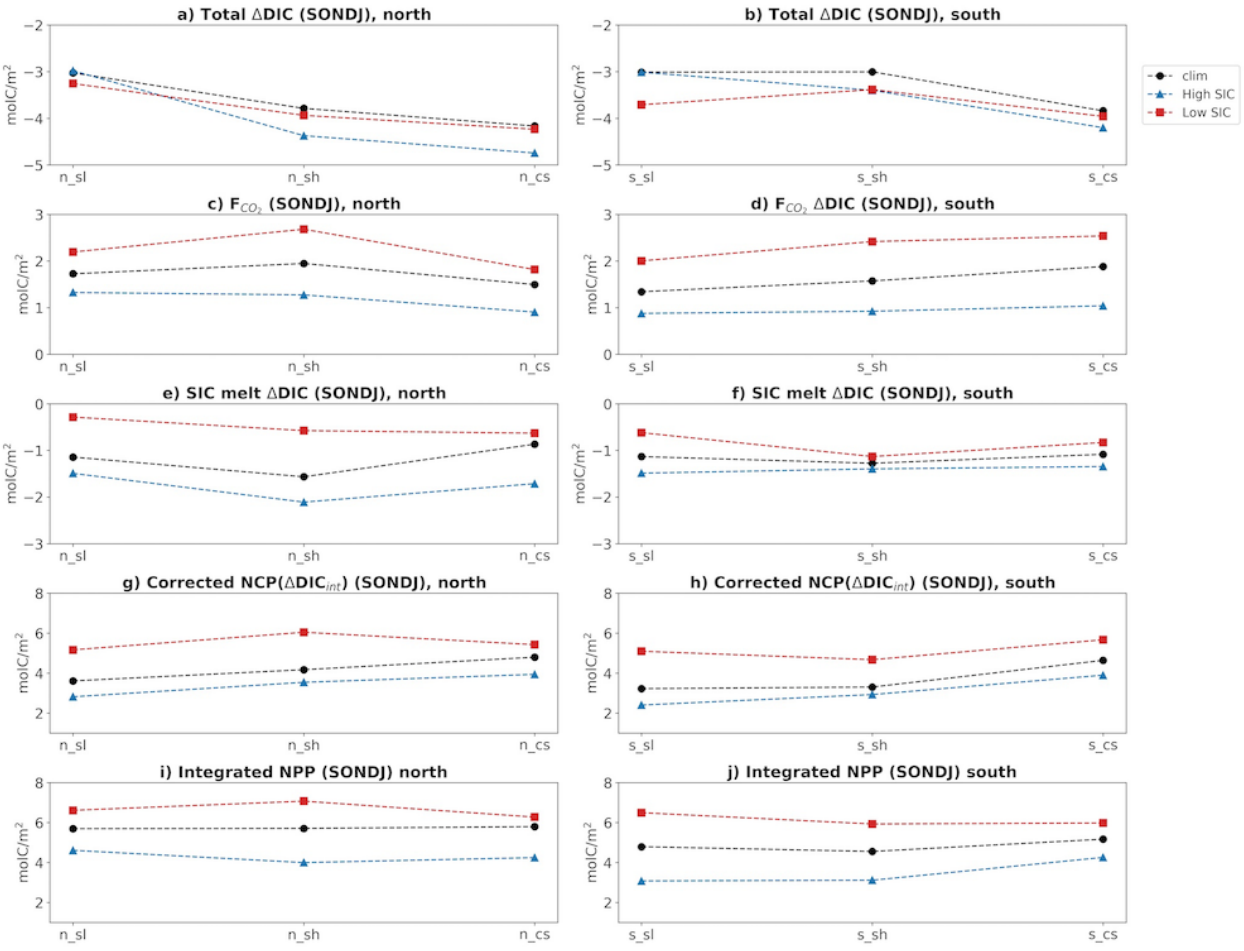

Figure 9: Seasonally integrated (between September and January) total vertically integrated DIC drawdown (a, b), air-sea CO_2 flux (c, d), effect of sea-ice melt on DIC concentration (e, f), DIC-derived NCP corrected for air-sea flux and sea ice melt (g, h) and NPP (I, j) for the northern (left) and southern (right) regions. The sign reflects the effect on the DIC inventory, so that positive F_{CO2} reflects a flux into the ocean and negative meltwater influence reflects dilution. Shown for climatology (black), years of early sea-ice retreat (red, 1998-1999, 2008-2009) and years of late sea-ice retreat (blue, 2004-2005, 2013-2014).

Evidence that both biological and physical processes can lead to anomalously high DIC drawdown is seen in the shelf sub-regions, where both years of early and late sea-ice retreat show more DIC drawdown than the climatological values. In years of early retreat, the low dilution by meltwater and increased DIC input by air-sea CO_2 fluxes is compensated by the higher NCP, which reaches values as high as 6.04 molC/m^2 in the northern shelf. In years of high SIC, however, low air-sea fluxes and higher meltwater content keep the DIC drawdown below climatological values despite the low NCP. The WAP is a sink of atmospheric carbon throughout the season in all years, but the amount of carbon the ocean uptakes depends on the duration of the ice-free season.

Years of high SIC show higher productivity in January, and overall higher DIC drawdown. If NPP and NCP are integrated over the spring and summer seasons, however, it is seen that this is because of the timing of the bloom associated with the effect of physics in the DIC drawdown, not because of higher productivity. While January high chlorophyll values are accompanied by larger DIC drawdowns, these effects are not directly linked, although they are both driven by the timing and magnitude of sea-ice melt. Years of low SIC also show more DIC drawdown than the climatology, driven by the higher NCP throughout the season. Despite the high NCP, years of early sea-ice retreat still show positive DIC anomalies in January. The anomalies, however, reflect the positive anomalies that are observed at the beginning of the season (Figure S5), which are also positive possibly due to increased mixing with DIC-rich subsurface waters under lower SIC.

4 Discussion and Conclusions

The MITgcm-REcoM2 model implemented for the west Antarctic Peninsula (WAP) is able to represent the main patterns observed in the phytoplankton bloom, such as higher concentrations onshore and progression of the bloom from north to south and offshore to onshore. The onshore-offshore chlorophyll gradient seen in the observations, however, is not as pronounced in the model simulation. Li et al. (2015) find that the annually integrated net community production (NCP) in the coastal areas is up to 8 times higher than what is observed offshore, and Vernet et al. (2008) finds that primary production ranges from 500-750 mgC/m^2d shoreward of the continental slope and from 250-400 mgC/m^2d over the slope region. In the model, January net primary production (NPP) is 2.25 times higher in the coastal region (compared to the slope) in the northern region, and 1.91 times higher in the southern region. Integrated over September-January, however, the whole grid shows comparable NPP.

Comparing chlorophyll values among the different datasets (cruise, satellite and model) is challenging given that the phytoplankton bloom in the WAP is highly variable and patchy, and there are gaps in the temporal and spatial coverage of the observations. Some of the discrepancies observed between datasets in the chlorophyll anomalies, therefore, are likely attributable to timing of the sampling. Dissolved inorganic carbon (DIC) anomalies in mid-summer, on the other hand, are the result of the cumulative effect of processes that took place throughout the season. The model captures well the climatological spatial pattern in the summer surface DIC field with larger seasonal drawdown and dilution onshore, and the model is able to reproduce much of the interannual variability seen in the DIC measurements from the Palmer LTER cruises. We can estimate the importance of biological and physical processes in driving DIC drawdown each year knowing that the model predicts higher seasonally integrated productivity in years of low SIC in accordance to the literature and that sea ice and MLD variability are well represented in the model (Schultz et al., 2020).

In years of early sea-ice retreat, both observations (satellite and cruise) and model data show lower chlorophyll concentrations in January compared to the climatology. While January NPP is also lower than climatology, seasonally integrated NPP (September to January) is higher, with a longer productive season due to light limitation being lifted earlier. Surface DIC

751 drawdown during the same period, however, is lower despite the increased NPP. This can be
752 attributed to the increased air-sea CO_2 fluxes and to decreased dilution by sea ice melt. Years of
753 late sea-ice retreat, on the other hand, show higher than climatological chlorophyll
754 concentrations in January in all the datasets analyzed. The model results indicate that these
755 years exhibit NPP higher than the climatology for January, but overall less seasonally integrated
756 NPP. The longer sea-ice season also leads to a smaller sink of atmospheric CO_2 and increased
757 influence of sea-ice melt, resulting in larger DIC drawdown between September and January.
758 Although it is hard to estimate when the bloom starts in the satellite data due to cloud
759 and sea-ice cover, in the model results the January chlorophyll concentration anomalies are a
760 result of the timing of the bloom; with late sea-ice retreat, the light limitation is lifted later in
761 the year and the bloom is closer to its peak in January, while early sea-ice retreat leads to an
762 earlier bloom and a weaker phytoplankton bloom in January, with the productivity decreasing
763 due to lower iron concentrations. The model results are consistent with DIC concentrations
764 deviating from the dilution curve, with lower concentrations than expected, in January during
765 years of high chlorophyll concentrations as found in Hauri et al. (2015), but our results suggest
766 that sea-ice melt also plays an important role in driving the seasonal DIC drawdown. Air-sea CO_2
767 fluxes have a much larger influence in counteracting the drawdown by biological activity in
768 years of early sea-ice retreat, due to longer ice-free season.
769 Since ocean dissolved iron (dFe) data is scarce, building initial and boundary conditions
770 for this micronutrient is a challenge. Given that iron is thought to be the limiting factor
771 offshore, and that complete iron limitation is not encountered in the model, we suspect that
772 the initial and boundary conditions overestimate dFe, which is supplied in excess in the offshore
773 region due to mixing with iron-rich subsurface waters. The lack of iron data is not only a
774 limitation to build reliable forcings for the model, but also to understand the mechanisms
775 governing the phytoplankton spatial and temporal variability in the WAP. The role of different
776 sources of dFe in the WAP biogeochemistry, therefore, is a question that requires future
777 research and increased field sampling.
778 Interannual variability of glacial sources of freshwater and dFe are also missing.
779 Although there is substantial melting of glacial waters on the continent, most of it freezes

780 before reaching the ocean (Van Wessem et al., 2016). The re-freezing of glacial melt impedes
781 the estimation of yearly runoff to the ocean, although a climatology can be obtained using the
782 mass balance over a larger time scale. Some of the discrepancies in chlorophyll concentration
783 between model and data are attributed to the lack of interannual variability in the glacial dFe
784 input. In 2011, Annett et al. (2017) found anomalously high dFe concentrations linked to
785 increased glacial meltwater, which in turn led to large and positive chlorophyll anomalies. This
786 was a warm year with very early sea-ice retreat, and the high chlorophyll concentration differs
787 from what is observed in other years of early SIC retreat (decreasing bloom by January). It
788 seems likely, therefore, that 2011 was indeed an anomalous year with high glacial input leading
789 to a sustained large bloom, and that the lack of interannual variability in the glacial inputs in the
790 model prevented it from representing the high bloom.
791 Sherrell et al. (2018) found that dFe near Palmer Deep (on the northern, coastal part of
792 the grid) is provided by sediment sources in coastal, shallower areas, which is then advected to
793 the shelf region. The authors also argue that the difference from the hypothesis proposed by
794 Annett et al. (2017), that dFe is mostly from glacial origin, could be due to regional differences
795 or due to errors in the data interpretation of Annett et al. (2017), which would be caused by
796 vertical mixing weakening the ^{18}O isotope signature used to estimate the origin of the
797 freshwater in that study. The model results suggest that sediment sources of dFe are important
798 in the coastal regions, and that part of the dFe in the northern shelf is also of sedimentary
799 origin. In the southern coast, however, glacial inputs and mixing with subsurface waters are
800 much larger sources of dFe than sediments. Our results, therefore, indicate that there are
801 regional differences in how iron is provided.
802 Since the model was able to reproduce much of the variability related to sea ice without
803 meltwater accounting for a source of dFe, we hypothesize that sea ice controls the blooms
804 through its influence in the physics of the ocean, but that it is not a significant source of dFe.
805 This conclusion stands even assuming that the magnitude of dFe sources are inaccurate, since
806 the physics of the model is sufficiently well represented to assume that the distribution of the
807 iron inputs is accurate.

The MITgcm-REcoM2 model results help to fill in the gaps in understanding the link between the ocean biology, chemistry and physics in the WAP earlier in the warm season, when the presence of clouds and sea ice hinders the acquisition of satellite and cruise data. Further quantification of each process in driving carbon sinks in the area rely on acquiring more spring and early summer data, and will greatly benefit from sampling efforts currently being deployed using moorings, buoys and gliders. Our results suggest that early sea ice retreat leads to an earlier bloom, with overall higher productivity during the summer season but lower chlorophyll concentrations in January. In years of late sea ice retreat, the bloom is closer to the peak in January, but the associated larger drawdown in DIC also reflects smaller air-sea CO_2 fluxes and increased sea ice melt. If the trends towards longer ice-free seasons and increased glacial melt persists, it is likely that the WAP will be a larger sink of atmospheric carbon with increased NCP.

Acknowledgements

The authors thank the scientists, students, technicians and ship crew, officers and captains involved in collecting Palmer LTER time series data. C. Schultz, S. Doney, M. Kavanaugh and O. Schofield acknowledge support by the US National Science Foundation (grant PLR-1440435), and C. Schultz and S. Doney acknowledge support from the University of Virginia. The MITgcm model is an open source model (mitgcm.org). The version used in this study, with added parameterizations and specific configurations, are on C. Schultz's github (https://github.com/crisoceano/WAP_MITgcm). Copies of the forcing files needed for the simulations are in four separate records on zenodo.org, under DOIs 10.5281/zenodo.3627365, 10.5281/zenodo.3627564, 10.5281/zenodo.3627742, and 10.5281/zenodo.4342315.

References

Annett, A.L., Skiba, M., Henley, S.F., Venables, H.J., Meredith, M.P., Statham, P.J., Ganeshram, R.S. (2015) Comparative roles of upwelling and glacial iron sources in Ryder Bay, coastal west Antarctic Peninsula, Marine Chemistry, 176, 21-33. Doi: 10.1016/j.marchem.2015.06.017

Annett, A.L., Fitzsimmons, J.N., Séguret, M.J.M., Lagerström, M., Meredith, M.P., Schofield, O. & Sherrell, R.M. (2017) Controls on dissolved and particulate iron distributions in surface waters of the Western Antarctic Peninsula shelf. *Marine Chemistry*, 196, 81-97. doi:10.1016/j.marchem.2017.06.004.

Arrigo, K.R., van Dijken, G., Long, M. (2008) Coastal Southern Ocean: A strong anthropogenic CO2 sink, Geophysical Research Letters, 35, L21602. Doi:10.1029/2008GL035624

Arrigo, K.R., van Dijken, G.L., Alderkamp, A.C., Erickson, Z.K., Lewis, K.M., Lowry, K.E., Joy-Warren, H.L., Middag, R., Nash-Arrigo, J.E., Selz, V., van de Poll, W. (2017) Early spring phytoplankton dynamics in the western Antarctic Peninsula. Journal of Geophysical Research – Oceans, 122, 9350-9369. Doi: 10.1002/2017JC013281

Brown, M. S., Munro, D. R., Feehan, C. J., Sweeney, C., Ducklow, H. W., Schofield, O. 2019. Enhanced oceanic CO_2 uptake along the rapidly changing West Antarctic Peninsula. Nature Climate Change. DOI: 10.1038/s41558-019-0552-3

Buessler, K.O., McDonnell, A.M.P., Schofield, O.M.E., Steinberg, D.K., Ducklow, H.W. (2010) High particle export over the continental shelf of the west Antarctic Peninsula, Geophysical Research Letters, 37, L22606. Doi:10.1029/2010GL045448

Carrillo, C.J., Smith, R.C., Karl, D.M. (2004) Processes regulating oxygen and carbon dioxide in surface waters west of the Antarctic Peninsula, Marine Chemistry, 84, 161-179. Doi:10.1016/j.marchem.2003.07.004

Carvalho, F., Kohut, J., Oliver, M. J., Sherrell, R. M., Schofield, O. (2016) Mixing and phytoplankton dynamics in a submarine canyon in the West Antarctic Peninsula. Journal of Geophysical Research DOI: 10.1002/2016JC011650

Comiso, J. C., (2017), Bootstrap Sea Ice Concentrations from Nimbus-7 SMMR and DMSP SSM/I-SSMIS, Version 3. Boulder, Colorado USA. NASA National Snow and Ice Data Center Distributed Active Archive Center. doi: 10.5067/7Q8HCCWS4I0R

Cook, A.J., Fox, A.J., Vaughan, D.G. & Ferrigno, J.G. (2005), Retreating glacier fronts on the Antarctic Peninsula over the past half-century. *Science*, 308, 541-544. doi:10.1126/science.1104235

Dierssen, H.M. and Smith, R.C. (2000), Bio- optical properties and remote sensing ocean color algorithms for Antarctic Peninsula waters. Journal of Geophysical Research: Oceans, 105(C11), 26301-26312. Doi: 10.1029/1999JC000296

Ducklow, H.W., W.R. Fraser, M.P. Meredith, S.E. Stammerjohn, S.C. Doney, D.G. Martinson, S.F. Sailley, O.M. Schofield, D.K. Steinberg, H.J. Venables, and C.D. Amsler (2013) West Antarctic Peninsula: An ice-dependent coastal marine ecosystem in transition, Oceanography, 26(3), 190-203. Doi:10.5670/oceanog.2013.62

Ducklow, H.W., A. Clarke, R. Dickhut, S.C. Doney, H. Geisz, K. Huang, D.G. Martinson, M.P. Meredith, H.V. Moeller, M. Montes-Hugo, O. Schofield, S.E. Stammerjohn, D. Steinberg, and W. Fraser (2012) The marine ecosystem of the West Antarctic Peninsula, in Antarctica Ecosystems: An Extreme Environment in a Changing World, 121-159pp, ed. A.D. Rogers, N.M. Johnston, E.J. Murphy, and A. Clarke, Wiley-Blackwell, ISBN: 978-1-4051-9840-0.

Ducklow, H.W., Stukel, M.R., Eveleth, R., Doney, S.C., Jickells, T., Schofield, O., Baker, A.R., Brindle, J., Chance, R., Cassar, N., (2018). Spring-summer net community production, new

production, particle export and related water column biogeochemical processes in the marginal sea ice zone of the West Antarctic Peninsula 2012-2014, Philosophical Transactions of the Royal Society A, 20170177. Doi:10.1098/rsta.2017.0177

Eveleth, R., Cassar, N., Sherrell, R.M., Ducklow, H., Meredith, M.P., Venables, H.J., Lin, Y., and Li, Z., (2017) Ice melt influence on summertime net community production along the Western Antarctic Peninsula, Deep Sea Research Part II: Topical Studies in Oceanography, 139, 89-102. Doi:10.1016/j.dsr2.1016.07.016

Eveleth, R., Cassar, N., Doney, S. C., Munro, D. R., Sweeney, C., (2017) Biological and physical controls on O2/Ar, Ar and pCO2 variability at the Western Antarctic Peninsula and in the Drake Passage, Deep Sea Research Part II: Topical Studies in Oceanography, 139, 77-88. Doi:10.1016/j.dsr2.2016.05.002

Garcia, H. E., R. A. Locarnini, T. P. Boyer, J. I. Antonov, O.K. Baranova, M.M. Zweng, J.R. Reagan, D.R. Johnson (2014) *World Ocean Atlas 2013, Volume 4: Dissolved Inorganic Nutrients (phosphate, nitrate, silicate).* S. Levitus, Ed., A. Mishonov Technical Ed.; NOAA Atlas NESDIS 76, 25 pp.

Garibotti, I.A., Vernet, M., Ferrario, M.E., (2005) Annually recurrent planktonic assemblages during summer in the seasonal ice zone west of the Antarctic Peninsula (Southern Ocean), Deep-Sea Research I, 52, 1823-1841. Doi:10.1016/j.dsr.2005.05.003

Gruber, N. and S.C. Doney, (2019) Modeling of ocean biogeochemistry and ecology, in *Encyclopedia of Ocean Sciences* (third edition), ed. J.K. Cochran, Elseiver, **5**, 291–302, doi:10.1016/B978-0-12-409548-9.11409-5

Hauck, J., Völker, C., Wolf-Gladrow, D.A., Laufkötter, C., Vogt, M., Aumont, O., Bopp, L., Buitenhuis, E.T., Doney, S.C., Dunne, J., Gruber, N., Hashioka, T., John, J., Le Quéré, C., Lima,

I.D., Nakano, H., Séréfian & R., Totterdell, I. (2015), On the Southern Ocean CO_2 uptake and the role of the biological carbon pump in the 21st century. *Global Biogeochemical Cycles*, 29, 1451-1470. doi:10.1002/2015GB005140

Hauck, J., Kohler, P., WolfGladrow, D., Volker, C., (2016) Iron fertilization and century-scale effects of open ocean dissolution of olivine in a simulated CO2 removal experiment, Environmental Research Letters, 11, 024007. Doi:10.1088/1748-9326/11/2/024007

Hauri, C., S.C. Doney, T. Takahashi, M. Erickson, G. Jiang, and H.W. Ducklow: 2015: Two decades of inorganic carbon dynamics along the West Antarctic Peninsula, Biogeosciences, 12, 6761-6779, doi:10.5194/bg-12-6761-2015

Holland, P.R., Bruneau, N., Enright, C., Losch, M., Kurtz, N.T. & Kwok, R. (2014), Modeled Trends in Antarctic Sea Ice thickness. *Journal of Climate*, 27, 3784-3801. doi:10.1175/JCLI-D-13-00301.1

Jones, E.M., Fenton, M., Meredith, M.P., Clargo, N.M., Ossebaar, S., Ducklow, H.W., Venables, H.J., and de Baar, H.J.W., (2017) Ocean acidification and calcium carbonate saturation states in the coastal zone of the West Antarctic Peninsula, Deep-Sea Research II, 139, 181-194. Doi: 10.1016/j.dsr2.2017.01.007

Kavanaugh, M.T., Abdala, F.N. Ducklow, H., Glover, D., Schofield, O., Stammerjohn, S., and Doney, S. C. (2015), Canyon effects on phytoplankton biomass and community structure along the Western Antarctic Peninsula. Marine Ecology Progress Series, 524:11-26. Doi: 10.3354/meps11189

Kavanaugh, M.T., Church, M.E, Davis, C.O., Karl, D.M., Letelier, R.M. and S.C. Doney (2018), ALOHA from the Edge: Reconciling three decades of in situ Eulerian observations and geographic variability in the North Pacific Subtropical Gyre, Frontiers of Marine Science. Doi: 10.3389/fmars.2018.00130

951
952 Key, R.M., Olsen, A., van Heuven, S., Lauvset, S.K., Velo, S., Lin, X., Schirnick, C., Kozyr, A.,
953 Tanhua, T., Hoppema, M., Jutterstrom, S., Steinfeldt, R., Jeansson, E., Ishi, M., Perez, F.F.,
954 Suzuki, T., Global Ocean Data Analysis Project, Version 2 (GLODAPv2), ORNL/CDIAC-162, NDP-
955 P093. Carbon Dioxide Information Analysis Center, Oak Ridge National Laboratory, US
956 Department of Energy, Oak Ridge, Tennessee, 2015.
957
958 Kim, H., Doney, S.C., Iannuzzi, R.A., Meredith, M.P., Martinson, D.G. & Ducklow, H.W. (2016),
959 Climate forcing for dynamics of dissolved inorganic nutrients at Palmer Station, Antarctica: An
960 interdecadal (1993–2013) analysis. *Journal of Geophysical Research: Biogeosciences*, *121* (9),
961 2369--2389. doi:10.1002/2015JG003311
962
963 Kim, H., Ducklow, H.W., Abele, D., Ruiz Barlett, E.M., Buma, A.G.J., Meredith, M.P., Rozema,
964 P.D., Schofield, O.M., Venables, H.J., and Schloss, I.R., (2018) Inter-decadal variability of
965 phytoplankton biomass along the coastal West Antarctic Peninsula. *Philosophical Transactions*
966 *of the Royal Society A: Mathematical, Physical and Engineering Sciences*, *376* (20170179). Doi:
967 10.1098/rsta.2017.0179.
968
969 Lauvset, S.K., Key, R.M., Olsen, A., van Heuven, S., Velo, A., Lin, X., Schirnick, C., Kozyr, A.,
970 Tanhua, T., Hoppema, M., JutterstrÖm, S., Steinfeldt, R., Jeansson, E., Ishii,M., Perez,F.F., Suzuki,
971 T., Watelet, S. (2016) A new global interior ocean mapped climatology: the 1˚ x 1˚ GLODAP
972 version 2. Earth System Science Data, 8, 325-340. Doi:10.5194/essd-8-325-2016
973
974 Legge, O.J., Bakker, D.C.E., Meredith, M.P., Venables, H.J., Brown, P.J., Jones, E.M. & Johnson,
975 M.T. (2017), The seasonal cycle of carbonate system processes in Ryder Bay, West Antarctic
976 Peninsula. *Deep Sea Research Part II: Topical Studies in Oceanography*, v. 139, 167-180. doi:
977 10.1016/j.dsr2.2016.11.006
978

Lenton, A., Tilbrook, B., Law, R.M., Bakker, D., Doney, S.C., Gruber, N., Ishii, M., Hoppema, M., Lovenduski, N.S., Matear, R.J., McNeil, B.I., Metzl, N., Mikaloff Fletcher, S.E., Monteiro, P.M.S., Rödenbeck, C., Sweeney, C., Takahashi, T., (2013) Sea-air CO2 fluxes in the Southern Ocean for the period 1990-2009, Biogeosciences, 10, 4037-4054, doi:10.5194/bg-10-4037-2013

Li, Z., Cassar, N., Huang, K., Ducklow, H.W., Schofield, O., (2016) Interannual variability in net community production at the Western Antarctic Peninsula region (1997-2014), Journal of Geophysical Research: Oceans, 121, 4748-4762. Doi:10.1002/2015JC011378

Long, M.C., Lindsay, K., Holland, M.M., (2015) Modeling photosynthesis in sea ice covered waters, Journal of Advances in Modeling Earth Systems, 07. Doi:10.1002/2015MS000436

Luo, C., Mahowald, N., Bond, T., Chuang, P.Y., Artaxo, P., Siefert, R., Chen, Y., Schauer, J., (2008) Combustion iron distribution and deposition, Global Biogeochemical Cycles, 22, GB1012. Doi: 10.1029/2007BG002964

Meredith, M.P. & King, J.C. (2005), Rapid climate change in the ocean west of the Antarctic Peninsula during the second half of the 20th century. *Geophysical Research Letters*, 32, 1-5. doi: 10.1029/2005GL024042

Montes-Hugo, M., Doney, S.C., Ducklow, H.W., Fraser, W., Martinson, D., Stammerjohn, S.E., Schofield, O., (2009). Science, 323, 5920, 1470-1473. Doi:10.1126/science.1164533

Regan, H.C., Holland, P.R., Meredith, M.P. & Pike, J. (2018), Sources, variability and fate of freshwater in the Bellingshausen Sea, Antarctica. *Deep-Sea Research Part I: Oceanographic Research Papers,* 133, 59-71. doi: 10.1016/j.dsr.2018.01.005

Schofield, O., Saba, G., Coleman, K., Carvalho A-F., Couto, N., Finkel, Z., Irwin, A., Kahl, A., Montes-Hugo, M.. Waite, N. (2017) Decadal variability phytoplankton community composition

in the coastal waters of a warming West Antarctic Peninsula. Deep Sea Research. doi/10.1016/j.dsr.2017.04.014

Schultz, C., Doney, S., Zhang, W.G., Regan, H., Holland, P., Meredith, M., and Stammerjohn, S., (2020) Modeling of the influence of sea ice cycle and Langmuir circulation on ocean surface mixed layer depth and freshwater distribution off the West Antarctic Peninsula. *Journal of Geophysical Research: Oceans*. Doi:10.1029/2020JC016109

Sherrell, R.M., Annett, A.L., Fitzsimmons, J.N., Roccanova, V.J., Meredith, M.P., (2018) A 'shallow bathtub ring' of local sedimentary iron input maintains the Palmer Deep biological hotspot on the West Antarctic Peninsula shelf. Philosophical Transactions of the Royal Society, A376: 20170171. Doi:10.1098/rsta.2017.0171

Stammerjohn, S.E., Martinson, D.G., Smith, R.C. & Ianuzzi, R.A. (2008), Sea ice in the western Antarctic Peninsula region: Spatio-temporal variability from ecological and climate change perspectives. *Deep-Sea Research Part II*, 55, 2041-2058. doi: 10.1016/j.dsr2.2008.04.026

Stammerjohn, S., Massom, R. A., Rind, D., & Martinson, D. (2012), Regions of rapid sea ice change: An inter-hemispheric seasonal comparison. *Geophysical Research Letters*, *39* (L06501). doi: 10.1029/2012GL050874

Stukel, M.R., Asher, E., Couto, N., Schofield, O., Strebel, S., Tortell, P., Ducklow, H.D., The imbalance of new and export production in the western Antarctic Peninsula, a potentially "leaky" ecosystem, Global Biogeochemical Cycles, 29, 1400-1420, 2015.

Takahashi, T., Sutherland, S.C., Chipman, D.W., Goddard, J.G., Ho, C., Newberger, T., Sweeney, C., Munro, D.R., (2014) Climatological distributions of pH, p$CO2$, total CO2, alkalinity, and CaCO3 saturation in the global surface ocean, and temporal changes at selected locations, Marine Chemistry, 164, 95-125. Doi:10.1016/j.marchem.2014.06.004

Van Wessem, J.M., Meredith, M.P., Reijmer, C.H., van den Broeke, M.R. & Cook, A.J. (2016), Characteristics of the modelled meteoric freshwater budget of the western Antarctic Peninsula, *Deep Sea Research Part II: Topical Studies in Oceanography*, 139, 31-39. doi:10.1016/j.dsr2.2016.11.001

Vernet, M., Martinson, D., Ianuzzi, R., Stammerjohn, S., Kozlowski, W., Sines, K., Smith, R. & Garibotti, I. (2008), Primary production within the sea ice zone west of the Antarctic Peninsula: I – Sea ice, summer mixed layer, and irradiance. *Deep-Sea Research Part II*, 55, 2068-2085. doi: 10.1016/j.dsr2.2008.05.021

Wanninkhok, R., (1992) Relationship between wind-speed and gas exchange over the ocean, Journal of Geophysical Research – Ocean, 97, 7373-7382. Doi:10.1029/92JC00188

Weston K, Jickells TD, Carson DS, Clarke A, Meredith MP, Brandon MA, Wallace MI, Ussher SJ, Hendry KR. (2013) Primary production export flux in Marguerite Bay (Antarctic Peninsula): Linking upper water-column production to sediment trap flux. Deep Sea Res. I 75, 52–66. doi:10.1016/j.dsr.2013.02.001